Available online at www.sciencedirect.com
ScienceDirect
Geochimica et Cosmochimica Acta 74 (2010) 6249–6262
Geochimica et Cosmochimica Acta
www.elsevier.com/locate/gca

Oxygen and iron isotope constraints on near-surface fractionation effects and the composition of lunar mare basalt source regions

Yang Liu [a,*], Michael J. Spicuzza [b], Paul R. Craddock [c], James M.D. Day [d], John W. Valley [b], Nicolas Dauphas [c], Lawrence A. Taylor [a]

[a] Planetary Geosciences Institute, Department of Earth & Planetary Sciences, University of Tennessee, Knoxville, TN 37996, USA
[b] Department of Geoscience, University of Wisconsin, 1215 W. Dayton St., Madison, WI 53706, USA
[c] Origins Laboratory, Department of the Geophysical Sciences, Enrico Fermi Institute, University of Chicago, Chicago, IL 60637, USA
[d] Department of Geology, University of Maryland, College Park, MD 20742, USA

Received 8 April 2010; accepted in revised form 5 August 2010; available online 12 August 2010

Abstract

Oxygen and iron isotope analyses of low-Ti and high-Ti mare basalts are presented to constrain their petrogenesis and to assess stable isotope variations within lunar mantle sources. An internally-consistent dataset of oxygen isotope compositions of mare basalts encompasses five types of low-Ti basalts from the Apollo 12 and 15 missions and eight types of high-Ti basalts from the Apollo 11 and 17 missions. High-precision whole-rock $\delta^{18}O$ values (referenced to VSMOW) of low-Ti and high-Ti basalts correlate with major-element compositions (Mg#, TiO_2, Al_2O_3). The observed oxygen isotope variations within low-Ti and high-Ti basalts are consistent with crystal fractionation and match the results of mass-balance models assuming equilibrium crystallization. Whole-rock $\delta^{56}Fe$ values (referenced to IRMM-014) of high-Ti and low-Ti basalts range from 0.134‰ to 0.217‰ and 0.038‰ to 0.104‰, respectively. Iron isotope compositions of both low-Ti and high-Ti basalts do not correlate with indices of crystal fractionation, possibly owing to small mineral-melt iron fractionation factors anticipated under lunar reducing conditions.

The $\delta^{18}O$ and $\delta^{56}Fe$ values of low-Ti and the least differentiated high-Ti mare basalts are negatively correlated, which reflects their different mantle source characteristics (e.g., the presence or absence of ilmenite). The average $\delta^{56}Fe$ values of low-Ti basalts (0.073 ± 0.018‰, $n = 8$) and high-Ti basalts (0.191 ± 0.020‰, $n = 7$) may directly record that of their parent mantle sources. Oxygen isotope compositions of mantle sources of low-Ti and high-Ti basalts are calculated using existing models of lunar magma ocean crystallization and mixing, the estimated equilibrium mantle olivine $\delta^{18}O$ value, and equilibrium oxygen-fractionation between olivine and other mineral phases. The differences between the calculated whole-rock $\delta^{18}O$ values for source regions, 5.57‰ for low-Ti and 5.30‰ for high-Ti mare basalt mantle source regions, are solely a function of the assumed source mineralogy. The oxygen and iron isotope compositions of lunar upper mantle can be approximated using these mantle source values. The $\delta^{18}O$ and $\delta^{56}Fe$ values of the lunar upper mantle are estimated to be 5.5 ± 0.2‰ (2σ) and 0.085 ± 0.040‰ (2σ), respectively. The oxygen isotope composition of lunar upper mantle is identical to the current estimate of Earth's upper mantle (5.5 ± 0.2‰), and the iron isotope composition of the lunar upper mantle overlaps within uncertainty of estimates for the terrestrial upper mantle (0.044 ± 0.030‰).

1. INTRODUCTION

Stable-isotope compositions of the major-element constituents to planetary mantles (e.g., O, Fe, Mg, Si, Ca) provide constraints on the genesis and differentiation of

* Corresponding author. Tel.: +1 865 974 6024; fax: +1 865 974 2368.
E-mail address: yangl@utk.edu (Y. Liu).

0016-7037/$ - see front matter © 2010 Elsevier Ltd. All rights reserved.
doi:10.1016/j.gca.2010.08.008

planetary bodies (e.g., O: Wiechert et al., 2001; Spicuzza et al., 2007; Fe: Wiesli et al., 2003; Poitrasson et al., 2004; Weyer et al., 2005; Dauphas et al., 2009a; Mg: Teng et al., 2010a; Si: Georg et al., 2007; Ca: Simon and DePaolo, 2010). In particular, oxygen isotope values of lunar rocks fall on the same oxygen-isotope mass-dependent fractionation line of Earth rocks (Clayton et al., 1971; Wiechert et al., 2001; Spicuzza et al., 2007), placing important limitations on models for the formation of the Earth–Moon system. The current view for the origin of the Moon, derived from dynamical simulations, is that a Mars-sized planetary embryo (Theia) impacted the proto-Earth and contributed 60–90% of its material to the Moon (Cameron, 1997; Canup and Asphaug, 2001). The constraints from oxygen isotopes would therefore imply: (1) that equilibration occurred between a magma ocean on Earth and a molten disk of proto-lunar materials through a common silicate-vapor atmosphere after the giant impact (Pahlevan and Stevenson, 2007), (2) the oxygen isotope composition of the proto-Earth and Theia were nearly identical (Wiechert et al., 2001), or (3) current models for Earth–Moon system formation require revision (Melosh, 2009).

Although the $\Delta^{17}O$ values between the Moon and Earth are indistinguishable, and can be explained through the diffusional exchange model of Pahlevan and Stevenson (2007), the $\delta^{18}O$ composition of the bulk Moon may be different from that of the bulk Earth (Spicuzza et al., 2007). Constraining the bulk Moon composition with respect to stable isotopes could offer information on the impactor (Theia) and thus shed light on the Earth–Moon formation.

Given the lack of lunar mantle samples and limited information on the internal structure of the Moon, a common approach for understanding the lunar upper mantle composition has been to measure the composition of mare basalts, which are partial melts of mantle sources. Previous petrological, geochemical and experimental studies of mare basalts have shown that they are derived from mineralogically and chemically heterogeneous lunar mantle sources (e.g., Taylor et al., 1991; Neal and Taylor, 1992; Papike et al., 1998; Shearer et al., 2006). These mantle sources are thought to represent different portions of the mantle cumulate pile generated during lunar magma ocean differentiation (e.g., Longhi, 1992; Papike et al., 1998; Shearer et al., 2006). The isotopic characteristics (e.g., O, Fe, Mg, and initial $^{87}Sr/^{86}Sr$, $^{143}Nd/^{144}Nd$, $^{176}Hf/^{177}Hf$) of low-Ti (1–6 wt% TiO_2) and high-Ti (>6 wt% TiO_2) basalts generally are quite distinct and are consistent with these models. Previous studies have shown that, relative to low-Ti basalts, high-Ti basalts have bulk $\delta^{18}O$ values lower by 0.20–0.25‰ (Clayton et al., 1971; Wiechert et al., 2001; Spicuzza et al., 2007; Hallis et al., 2009), and bulk $\delta^{56}Fe$ values higher by 0.1–0.2‰ (Wiesli et al., 2003; Poitrasson et al., 2004; Weyer et al., 2005).[1] The chemical/mineralogical variations between and within these basalts complicate estimation of the stable-isotope composition (especially O, Fe) of the lunar mantle. Poitrasson et al. (2004) estimated the Fe isotope composition of the Moon by directly averaging all different types of basalts. This result was later questioned (Weyer et al., 2005) as the volumetric proportions of the various mantle sources are not taken into consideration.

To further understand lunar mantle differentiation and constrain the lunar mantle composition, we report coupled high-precision oxygen and iron isotope data for low-Ti and high-Ti basalt samples, many of which have not been studied previously for these isotope systems. These new oxygen isotope data are interpreted together with previously published oxygen isotope data of low-Ti and high-Ti basalts from the same laboratory (Spicuzza et al., 2007). The extended dataset covers Apollo 11 and 17 high-Ti basalts (8.6–13.5 wt% TiO_2) and Apollo 12 and 15 low-Ti basalts (1.7–5.1 wt% TiO_2). Iron isotope data are reported for low-Ti and high-Ti basalts also measured for their oxygen isotope compositions. The oxygen and iron isotope data are compared with major-element chemistry in order to assess the effect of crystal fractionation and to help constrain the oxygen and iron isotope composition of the lunar upper mantle.

2. SAMPLES AND ANALYTICAL METHODS

2.1. Samples

Mare basalts are distinguished using their bulk compositions, such as TiO_2, Al_2O_3, and K_2O (Neal and Taylor, 1992). On the basis of bulk-rock TiO_2 contents, mare basalts are divided into very-low-Ti (<1 wt% TiO_2), low-Ti (1–6 wt% TiO_2), and high-Ti basalts (>6 wt% TiO_2). The mare basalt samples chosen for this study are representative of the most abundant types, and include eleven low-Ti basalts from the Apollo 12 and 15 sites, and eight high-Ti basalts from the Apollo 11 and 17 collections (Table 1). Using the definition of Neal and Taylor (1992), all mare basalts in this study are low-Al (<11 wt% Al_2O_3) and low-K (<0.2 wt% K_2O) with the exception of Apollo 11 Type A (high-K, low-Al) sample 10057 (0.26 wt% K_2O).

The low-Ti basalts include five subgroups: Apollo 12 olivine, pigeonite, and ilmenite basalts, and Apollo 15 olivine-normative and quartz-normative basalts, which are distinguished on the basis of modal and normative mineralogy. Rhodes et al. (1977) suggested that Apollo 12 olivine and pigeonite basalts are co-magmatic. A recent study on Apollo 15 olivine-normative and quartz-normative basalts suggests that the more mafic members of the Apollo 15 olivine-normative basalts could be linked by crystal fractionation to less mafic, quartz-normative basalts from the same site (Schnare et al., 2008). The alternative view is that the major- and trace-element chemistry of most low-Ti basalts results from their derivation from several distinct mantle sources (see Papike et al., 1998).

Ten subgroups of high-Ti basalts have been defined based on differences in mineralogy (e.g., presence of olivine or tridymite/cristobalite) and trace-element characteristics

[1] The notation $\delta^{18}O$ is defined as $[(^{18}O/^{16}O)_{sample}/(^{18}O/^{16}O)_{VSMOW} - 1] * 1000$, where VSMOW is the international standard (Vienna Standard Mean Ocean Water). The $\delta^{56}Fe$ and $\delta^{57}Fe$ notations are defined as $[(^{\#}Fe/^{54}Fe)_{sample}/(^{\#}Fe/^{54}Fe)_{IRMM\text{-}014} - 1] * 1000$, where IRMM-014 is the international standard (Institute for Reference Materials and Measurements) and # is 56 or 57.

Table 1
Oxygen and iron isotope data and selected major-element compositions for lunar mare basalts.

Samples	Rock type[a]	$\delta^{18}O$[b]	1SD[b]	$\Delta^{17}O$[b]	*n*-O[b]	$\delta^{56}Fe$[c]	95% ci[c]	$\delta^{57}Fe$[c]	95% ci[c]	*n*-Fe[c]	Mg#	TiO_2 (wt%)
Low-Ti mare basalts; this study												
12002,188	Olivine basalt	5.57	0.07		2	0.103	0.038	0.158	0.047	1	55.4	2.59
12052,153	Olivine basalt	5.73	0.05		2	0.091	0.034	0.137	0.047	1	43.5	3.30
12021,286	Pigeonite basalt	5.78	0.05		2	0.062	0.018	0.082	0.025	3	39.9	3.53
12051,37	Pigeonite basalt	5.65	0.07		2	0.104	0.029	0.157	0.050	1	38.6	4.63
12064,87	Ilmenite basalt	5.78	0.07		2						38.7	3.57
15555,87	Olivine-norm basalt	5.62	0.00		2						46.0	2.19
15556,194	Olivine-norm basalt	5.73	0.07		2						40.3	2.60
15557,26	Olivine-norm basalt	5.72	0.05		2						43.1	2.54
15075,52	Quartz-norm basalt	5.79	0.12		2	0.049	0.024	0.056	0.033	2	42.8	1.81
15476,7	Quartz-norm basalt	5.71	0.05		2						43.2	1.82
15495,129	Quartz-norm basalt	5.76	0.05		2						43.2	1.88
Low-Ti mare basalt; Spicuzza et al. (2007)												
12018,43	Olivine basalt	5.662		−0.002	1						55.1	2.63
12063,321	Olivine basalt	5.694		−0.005	1						45.8	4.74
12052,110	Olivine basalt	5.813	0.016	0.009	2						43.5	3.30
12051,48	Pigeonite basalt	5.722		0.009	1						38.6	4.63
12056,18	Ilmenite basalt	5.715	0.090	0.019	2						43.7	5.07
15016,221	Olivine-norm basalt	5.616	0.016	0.020	2	0.067	0.029	0.122	0.050	1	47.5	2.28
15555,950[d]	Olivine-norm basalt	5.443	0.002	0.015	2						46.0	2.19
15555,955[d]	Olivine-norm basalt	5.631	0.212	0.004	2	0.073	0.029	0.104	0.050	1	46.0	2.19
15555,958[d]	Olivine-norm basalt	5.769	0.054	−0.020	2						46.0	2.19
15596,24	Quartz-norm basalt	5.602		0.021	1						n.a.	n.a.
15475,187	Quartz-norm basalt	5.682		0.014	1	0.038	0.028	0.067	0.038	1	43.8	1.74
15499,154	Quartz-norm basalt	5.693	0.029	0.011	2						45.4	1.78
High-Ti mare basalts; this study												
10044,116	B1-type basalt	5.61	0.07		2						37.9	9.09
10045,30	B3-type basalt	5.70	0.08	0.015	2						43.3	10.6
10057,183	A-type basalt; high-K	5.68	0.06	0.006	2						42.3	10.6
71539,17	A-type basalt	5.72	0.07		2	0.212	0.036	0.329	0.045	1	33.7	8.60
75015,1	A-type basalt	5.66	0.05		2	0.210	0.034	0.299	0.047	1	34.3	9.13
75035,149	A-type basalt	5.66	0.07		2						38.8	9.42
70035,9	U-type basalt	5.40	0.07		2	0.142	0.023	0.188	0.034	2	49.1	13.0
75075,158[d]	B1-type basalt	5.54	0.05		2						47.8	13.4
High-Ti mare basalts Spicuzza et al. (2007)												
70135,98	A-type basalt	5.591	0.102	0.026	2						48.0	13.5
75075,171[d]	B1-type basalt	5.335	0.084	0.018	2	0.217	0.030	0.330	0.048	1	47.8	13.4
70215,322	B2-type basalt	5.529		−0.004	1	0.171	0.028	0.261	0.038	1	44.4	12.8
74255,185	C-type basalt	5.407	0.087	0.008	2	0.182	0.029	0.283	0.050	1	51.7	12.5
74275,240	C-type basalt	5.400		−0.007	1						50.4	12.3
70017,524	U-type basalt	5.578	0.010	0.009	2	0.205	0.029	0.350	0.050	1	48.1	13.0
70035,180	U-type basalt	5.367	0.030	0.015	2						49.1	13.0

[a] Rock types for Apollo 11 and 17 high-Ti basalts were defined using the classification scheme presented in Rhodes et al. (1976), Rhodes and Blanchard (1980), and Neal et al. (1990).

[b] *n*-O: number of replicate analyses. 1SD: 1 standard variation of replicates. The 2SD of oxygen isotope analyses is ±0.10‰, based on 22 analyses of the garnet standard (UWG-2). $\Delta^{17}O_{sample}$ is calculated as described in Spicuzza et al. (2007).

[c] *n*-Fe is the number of replicate analyses. The 95% CI (confidence interval) obtained on standard IRMM-014 was reported for samples with one aliquot ($n = 1$). For samples with 2–3 replicate analyses, the weighted average value of replicates and its 95% confidence interval are reported here. Weights for the calculation are 95% confidence intervals of individual analyses.

[d] Sample 75075 display a larger variation in $\delta^{18}O$ among different sub-samples; possibly a result of heterogeneous mineral distribution as demonstrated for 15555 (Spicuzza et al., 2007).

(e.g., REE abundances, La/Sm, Sm/Yb; see Neal and Taylor, 1992). Three subgroups (Apollo 11 Type B1, B3, and Apollo 17 Type C) were suggested to have formed from the same mantle source (Snyder et al., 1990; Jerde et al., 1994). High-Ti mare basalts have been demonstrated to represent at least eight distinct mantle source regions

(e.g., Rhodes et al., 1976; Beaty and Albee, 1978; Rhodes and Blanchard, 1980). In all cases, examination of major- and trace-element trends within the Apollo 11 and 17 subgroups highlights the pronounced effect of near-surface crystal fractionation (e.g., Rhodes et al., 1976; Beaty and Albee, 1978; Neal et al., 1990).

Mare basalts types analyzed for their oxygen isotope composition in this study (not previously examined by Wiechert et al. (2001) or Spicuzza et al. (2007)) include Apollo 11 Type A, B1, and B3, and Apollo 17 Type A basalts. Iron isotope measurements were conducted on four subgroups of low-Ti and four subgroups of high-Ti basalts, including six samples for which iron isotope data have not been previously reported. Whole-rock, major- and trace-element compositions of most of these samples are tabulated in Meyer (2004–2008) and Neal (2008). The average major-element compositions of mare basalts were obtained from these compiled datasets (see Supporting Online Material). The mare basalts studied here span a wide range of Mg# (55–34) and TiO_2 contents (1.7–13.5 wt%) (Table 1).

2.2. Measurement of oxygen isotopes

Oxygen isotope analyses were performed at the Stable Isotope Laboratory, Department of Geoscience, University of Wisconsin, Madison. Laser fluorination oxygen three-isotope measurements were made on two samples (10045, 10057) following the procedures outlined in Spicuzza et al. (2007). The deviation ($\Delta^{17}O$) of samples from the terrestrial fractionation line (TFL) was calculated using the slope (λ) of 0.5259 determined by Spicuzza et al. (2007).

High-precision $^{18}O/^{16}O$ measurements on the majority of samples were measured using an airlock method (Spicuzza et al., 1998). The airlock allows direct laser fluorination of powders without pre-fluorination or fusion of the powder to a glass bead. For coarse-grained or heterogeneous chips, the samples were ground to a finer-grain size and carefully split to yield 50–100 mg, which was then further powdered for the measurement of $\delta^{18}O$. The reported $\delta^{18}O$ values of lunar basalts were standardized using 4–8 analyses of the UWG-2 garnet standard (Valley et al., 1995). During the course of measurement, the 2SD external reproducibility derived from 22 analysis of $\delta^{18}O$ in the UWG-2 garnet standard was ±0.10‰.

2.3. Measurement of iron isotopes

The protocol for the preparation of iron in geologic materials for isotope analysis is described in detail in Dauphas et al. (2004, 2009b) and Craddock and Dauphas (2010) and summarized below. Approximately 10 mg of whole-rock powder from a larger batch of homogeneous powder was digested using concentrated HF–HNO_3–$HClO_4$ and HNO_3–HCl–$HClO_4$ acid mixtures. The fully dissolved sample was evaporated to dryness following each acid digestion and subsequently taken up in ultra-pure 6 M HCl for chromatographic separation of Fe. Iron solutions were purified on disposable Bio-Rad Poly-Prep columns, filled with 1 mL of conditioned AG1-X8 200–400 mesh chloride-form resin. Sample solutions were loaded on the column in 6 M HCl. At this molarity, Fe is quantitatively retained on the resin. Matrix elements were eluted in 8 mL of 6 M HCl, added to the column in increments of 0.5, 0.5, 1, 2, and 4 mL. Iron was then eluted in 9 mL of 0.4 M HCl, added in increments of 0.5, 0.5, 1, 3, and 4 mL. The chromatographic separation of Fe was performed twice, each using new columns and resin. Dauphas et al. (2004, 2009b) have demonstrated 100% yield and negligible iron isotopic fractionation using this purification scheme. The Fe eluate was evaporated to dryness, taken up in ~100 μL of 15.3 M HNO_3, evaporated to dryness again to eliminate chlorine, and dissolved in 10 mL of 0.3 M HNO_3, for isotope analysis. The standard (IRMM-014 or IRMM–524a pure Fe metal; Taylor et al., 1992; Craddock and Dauphas, 2010) and blank solutions used for isotopic calibration and background corrections, respectively, are prepared from the same stock of 0.3 M HNO_3 to ensure exact matching of acid molarity, which is critical for accurate isotope analysis at the precisions attained (±0.03‰ for $\delta^{56}Fe$ and ±0.05‰ for $\delta^{57}Fe$ at the 95% confidence level).

Iron isotope analyses were performed with a Thermo Scientific Neptune multi-collector inductively coupled plasma mass spectrometer (MC-ICPMS) at the University of Chicago. Solutions were introduced into the mass spectrometer using a dual cyclonic Scott-type spray chamber. Isotope measurements were performed in medium mass resolution mode, whereby Fe^+ peaks are resolved from isobaric ArN^+, ArO^+, and $ArOH^+$ interferences as flat-topped plateaus on the low-mass shoulder of argide peaks (Weyer and Schwieters, 2003). Potential isobaric interferences from Cr and Ni were monitored on masses $^{53}Cr^+$ and $^{64}Ni^+$ and subtracted from Fe signals as necessary; such corrections were always negligible. Instrumental background (on-peak zero) on iron isotopes was determined by measurement of a clean 0.3 M HNO_3 solution (blank) at the beginning of each analytical session and subtracted from all standard and sample data. Instrumental mass fractionation was corrected using standard-sample bracketing (e.g., Belshaw et al., 2000; Albarède and Beard, 2004). Iron isotope variations are expressed in δ notation relative to IRMM-014, a reference material with an iron isotope composition identical to chondrites (Dauphas and Rouxel, 2006; Craddock and Dauphas, 2010).

Typical analytical uncertainties associated with the measurement of $\delta^{56}Fe$ and $\delta^{57}Fe$ values are ±0.03‰ and ±0.05‰ (95% confidence interval), respectively (Dauphas et al., 2009b). In the following text, quoted uncertainties are 95% confidence intervals for each independent analysis, or as a weighted uncertainty of two or more replicate analyses carried out on different analytical sessions.

3. RESULTS

3.1. Oxygen isotope ratios

Oxygen isotope ($\delta^{18}O$) compositions of low-Ti and high-Ti basalts analyzed in this study are listed in Table 1 with selected major-element contents. While the bimodal distribution of $\delta^{18}O$ values between high-Ti and low-Ti basalts

has been reported previously (Wiechert et al., 2001; Spicuzza et al., 2007), a significant feature of the new data is the correlation of the measured $\delta^{18}O$ values with major-element compositions (e.g., Mg#, Al_2O_3) within both low-Ti and high-Ti basalts (Table 1 and Fig. 1). Since the total oxygen isotope variability in lunar basalts is small, these new data are combined only with high-precision data obtained in the same laboratory (i.e. Spicuzza et al., 2007) to avoid confounding effects from inter-laboratory biases. The $\delta^{18}O$ value of high-Ti basalts increases by ~0.3‰ as Mg# decreases from 53 to 34. Differences among these high-Ti populations are distinct at the >99% level of confidence using the Student's *t*-test. A linear fit of $\delta^{18}O$ versus Mg# of all high-Ti basalts generates a slope of −0.016 that is significantly larger than the uncertainty (±0.004) of the fit slope. Low-Ti basalts display a similar but smaller increase in $\delta^{18}O$ (~0.15‰) with decreasing Mg# and with increasing Al_2O_3 (Fig. 1). Although the difference in $\delta^{18}O$ between high Mg# and low Mg# low-Ti basalt samples is comparable to the analytical uncertainty for a single analysis (±0.1‰), $\delta^{18}O$ and Mg# of all low-Ti basalts follow a trend with a slope of -0.010 ± 0.005 (Fig. 2). The magnitude of this variation is consistent with crystal fractionation (see Section 4). To examine which processes among magma mixing, partial melting, and crystal fractionation may have fractionated the oxygen isotopes of these basalts, measured $\delta^{18}O$ values are plotted versus CI-chondrite normalized La/Sm values (Fig. 3). Low-Ti and high-Ti basalts plot in distinct fields, except for the high-K, high-Ti sample 10057 (Apollo 11 Type A), which plots in the low-Ti basalt field (Fig. 3). The La/Sm value and high-K content of sample 10057 are consistent with assimilation of KREEP in Apollo 11 Type A mantle source (e.g., Jerde et al., 1994).

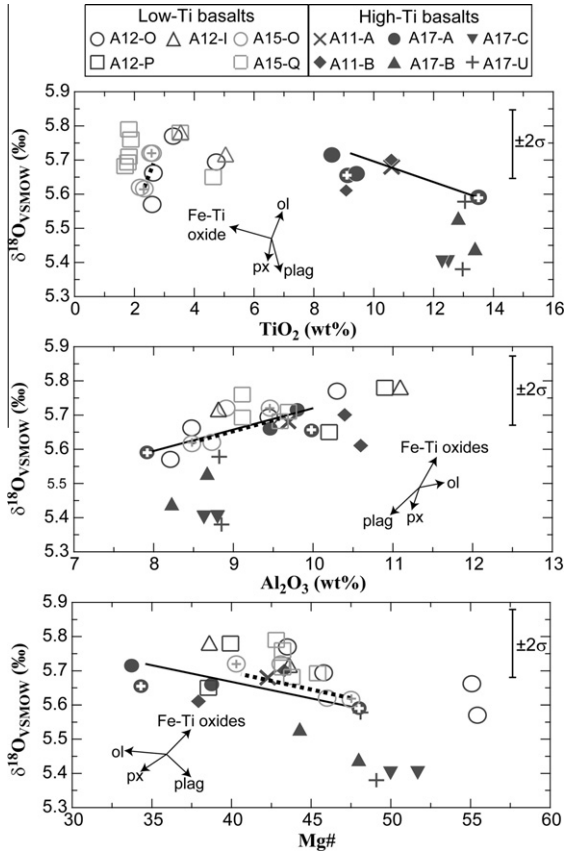

Fig. 1. Whole-rock oxygen isotope compositions of mare basalts versus their bulk compositions. Solid and dashed lines show the liquid compositions from Tables 2 and 3, respectively. Symbols with a cross in the center represent samples used in the calculation. The vector lines (relative to an arbitrary origin) schematically show the direction of an evolving melt composition after removing the corresponding mineral phase. Different symbols are used for different subgroups, with A12-O, A12-P and A12-I standing for olivine-, pigeonite-, and ilmenite-basalts from the Apollo 12 mission, A15-O and A15-Q stand for olivine- and quartz-norm basalts from the Apollo 15 mission. The Apollo 11 Type B1 and B3 basalts are plotted as one symbol (A11-B). The Apollo Type B1 and B3 basalts are also plotted as one symbol (A17-B). For clarity, the precision of a single analysis of $\delta^{18}O$ (2SD) is shown in the upper right corner of all three figures.

3.2. Iron-isotope ratios

The $\delta^{56}Fe$ and $\delta^{57}Fe$ values of 15 mare basalts analyzed here (Table 1 and Fig. 4) form a tight zero-intercept linear trend with a slope of 1.503 ± 0.055 (95% confidence interval), which agrees with slopes previously determined for mass-dependent fractionation (Malinovsky et al., 2003; Dauphas et al., 2010). These and other $\delta^{56}Fe$ and $\delta^{57}Fe$ for lunar basalts (e.g., Wiesli et al., 2003; Poitrasson et al., 2004) suggest that iron isotope variations in magmatic rocks from the Earth and Moon follow similar mass-dependent fractionation lines.

Bulk iron-isotope ratios ($\delta^{56}Fe$) of low-Ti basalts are lower than those of high-Ti basalts by 0.04–0.18‰ (Table 1, and Figs. 4 and 5). The new Fe isotope data compare well with literature data (Wiesli et al., 2003; Poitrasson et al., 2004; Weyer et al., 2005). Our data suggest that there are no significant correlations between $\delta^{56}Fe$ values and major-element compositions within low-Ti and high-Ti basalts (Fig. 5). The $\delta^{56}Fe$ values of all subgroups of high-Ti basalts are similar. Low-Ti and high-Ti basalts form a linear trend in $\delta^{56}Fe$ versus TiO_2 (Fig. 5a), but they form

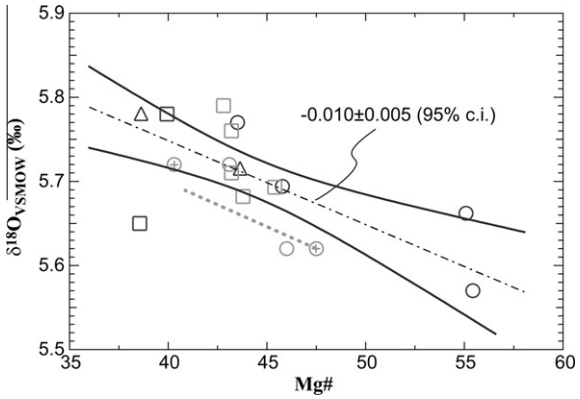

Fig. 2. Linear fit (dot-dashed line) of $\delta^{18}O$ and Mg# of all low-Ti mare basalts. The curved solid lines are the 95% confidence interval of the fit. Dotted line is the calculated trend for olivine-norm Apollo 15 basalts (Table 3). Symbols are the same as in Fig. 1.

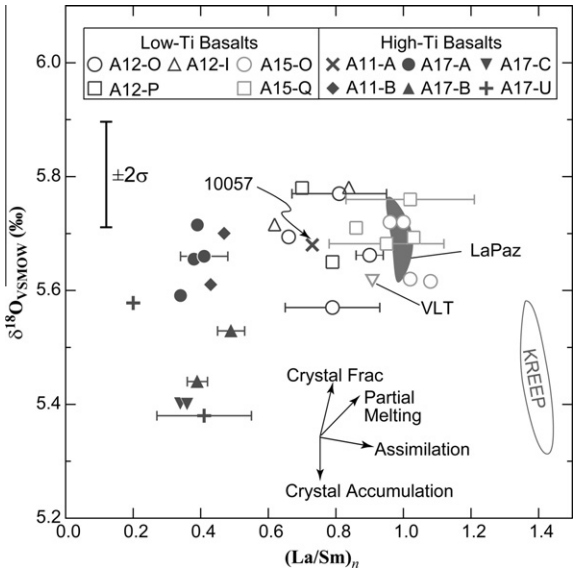

Fig. 3. $\delta^{18}O$ versus CI-chondrite normalized La/Sm. The $\delta^{18}O$ values of very-low-Ti and KREEP basalts are from Wiechert et al. (2001). Because of the broadly similar compatibility (Sm is slightly more compatible in silicates), La/Sm is a good indicator of the source signature. Trace element data are from an individual report where possible (Neal, 2001, Day et al., 2006). The average values from the Lunar Basalt Database (Neal, 2008) were used if not available. The 1σ standard deviation for the averaged La/Sm values is shown as error bars. Vectored lines schematically show the direction of melt affected by crystal fractionation (FC), partial melting (PM), assimilation/mixing (AsM), and crystal accumulation (CA). The large scattering in $(La/Sm)_n$ of low-Ti basalts is partly a result of relatively large uncertainties associated with the low abundances in small sample aliquots.

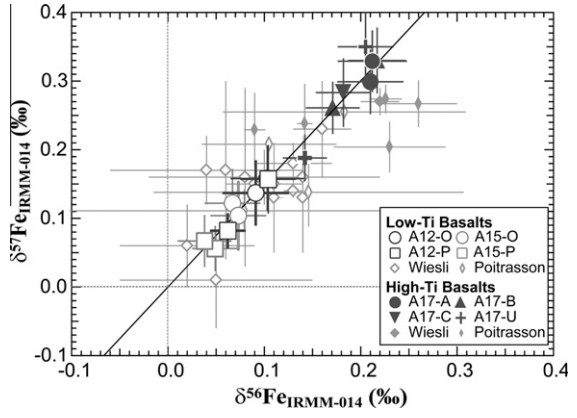

Fig. 4. Three iron isotopes plot of lunar mare basalts. Symbols for samples from this study are the same as in Fig. 1. The solid line is the linear fit through the origin of our data for mare basalts and has a slope of 1.503 ± 0.055. The 2σ uncertainties for each symbol are plotted. The $\delta^{57}Fe$ and $\delta^{56}Fe$ values of other mare basalts by Wiesli et al. (2003) and Poitrasson et al. (2004) are also reported here. The $\delta^{56}Fe$ values of Poitrasson et al. (2004) are calculated from their reported $\delta^{57}Fe/^{54}Fe$ and $\delta^{57}Fe/^{56}Fe$ values. Data of Weyer et al. (2005) are not plotted as they only reported $\delta^{56}Fe$ values.

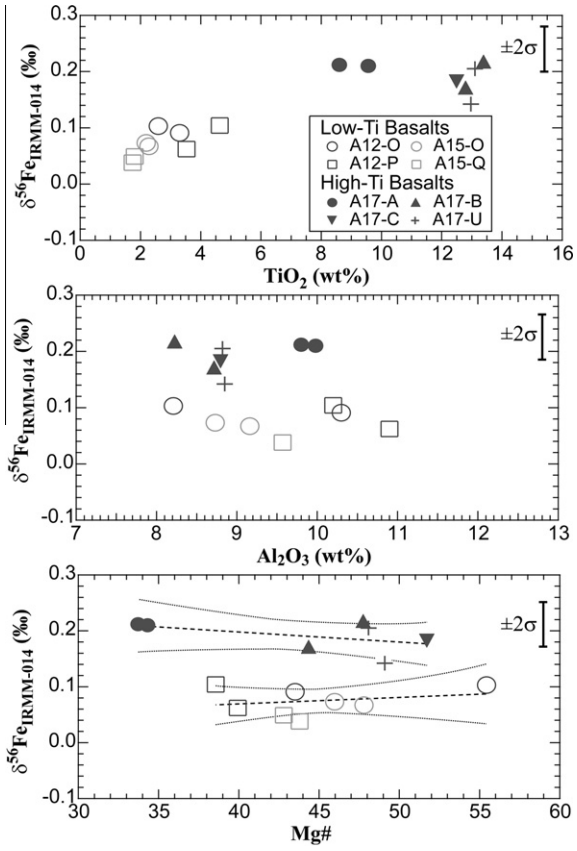

Fig. 5. Iron-isotope ratios of lunar mare basalts versus their whole-rock compositions from this study. Symbols are the same as in Fig. 1. Dashed lines are linear regression lines for $\delta^{56}Fe$ and Mg# of high-Ti and low-Ti basalts, respectively, weighted by the uncertainty of the data. The dotted curves plot the 95% confidential intervals of both fits. The fact that all $\delta^{56}Fe$ values of the high-Ti basalts lie in the envelope defined by the 95% confidential interval, and the fit slope is insignificant compared to its uncertainty (-0.002 ± 0.002 for high-Ti and 0.001 ± 0.002 for low-Ti), demonstrates that $\delta^{56}Fe$ of low-Ti and high-Ti basalts is independent of major-element compositions.

sub-parallel trends in $\delta^{56}Fe$ versus Al_2O_3 and Mg# (Fig. 5b and c). The average $\delta^{56}Fe$ values of low-Ti and high-Ti basalts analyzed in this study are $0.073 \pm 0.018‰$ (2SE, $n = 8$) and $0.191 \pm 0.020‰$ (2SE, $n = 7$), respectively. These average values show excellent agreement with average values of low-Ti ($0.105 \pm 0.029‰$, $n = 9$) and high-Ti ($0.205 \pm 0.036‰$, $n = 8$) basalts determined in previous studies (Wiesli et al., 2003; Poitrasson et al., 2004; Weyer et al., 2005).

3.3. Combined oxygen-iron isotope systematics

Low-Ti and high-Ti basalts exhibit striking differences in the plot of $\delta^{56}Fe$ versus $\delta^{18}O$ (Fig. 6). A notable feature of this plot is that high-Ti basalts with 8–12 wt% TiO_2 ("fractionated TiO_2") do not plot between the fields defined by high-Ti basalts with >12 wt% TiO_2 and low-Ti basalts. "Fractionated" high-Ti basalts are considered to have formed through significant crystal fractionation processes (Rhodes et al., 1976; Neal et al., 1990; see Section 4).

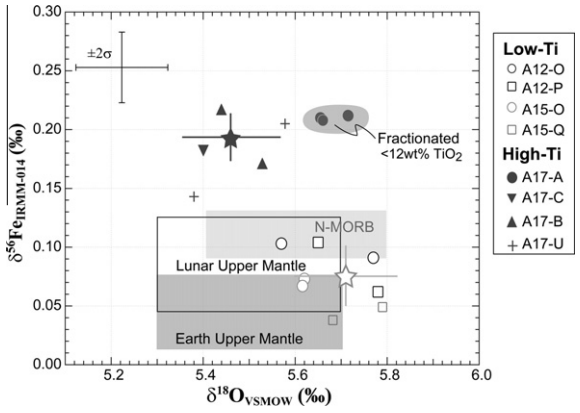

Fig. 6. Whole-rock δ^{56}Fe and δ^{18}O values of mare basalts from this study. Symbols are the same as in Fig. 1. Stars are the average of the least differentiated low-Ti and high-Ti samples. Error bars on the average values show the 2SE of the average. The light gray field labels the range of whole-rock δ^{56}Fe and δ^{18}O values of N-MORB. Inferred δ^{56}Fe and δ^{18}O ranges of lunar upper mantle are plotted as the open field. The range of δ^{56}Fe and δ^{18}O values of Earth's upper mantle (Eiler, 2001; Dauphas et al., 2010) is plotted in the darker gray rectangle.

High-Ti mare basalts contain higher δ^{56}Fe and lower δ^{18}O than those of normal MORB (N-MORB) (Eiler, 2001; Dauphas et al., 2009a). Low-Ti basalts plot between fields of the N-MORB and the Earth's upper mantle (Fig. 6).

4. DISCUSSION

Our results reveal several chemical characteristics within and between low-Ti and high-Ti mare basalts including correlations between oxygen isotope values and major-element compositions and a broadly negative correlation between oxygen and iron isotope values. In the following discussion, we will first discuss and model oxygen isotope variations within low-Ti and high-Ti basalts, then estimate the oxygen and iron isotope compositions of low-Ti and high-Ti mantle sources, and finally calculate δ^{18}O and δ^{56}Fe for the lunar upper mantle based on current constraints for these isotope systems.

4.1. Oxygen variations within low-Ti and high-Ti groups: near-surface fractionation effects

The small variations of δ^{18}O within the low-Ti and the high-Ti groups are possibly due to one or more of the following processes: heterogeneous mantle sources, varying degrees of partial melting, magma assimilation or mixing, and/or crystal fractionation. Some of these igneous processes can be distinguished by using the ratio of trace elements of similar compatibility/incompatibility (Eiler et al., 2000). Here, we use the La/Sm ratio of mare basalts because these elements show similar incompatible behavior and these data are readily available for mare basalts in the literature. Samples affected by assimilation or magma mixing, will fall into a linear trend between end-members. Samples affected only by partial melting will follow a trend of decreasing La/Sm with increasing degrees of partial melting (La is slightly more incompatible than Sm). Samples affected only by crystal fractionation will form a nearly vertical line in δ^{18}O–La/Sm space. As shown in Fig. 3, mare basalts from a given subgroup of mare basalt fall along nearly vertical trends in δ^{18}O–La/Sm space, consistent with crystal fractionation effects observed in major-elements.

The effect of crystal fractionation on oxygen isotope compositions is estimated using a chemical and oxygen-isotope mass-balance calculation. The MELTS program (Ghiorso and Sack, 1995) is frequently applied in such calculations for terrestrial magmatic systems, but could not be used here as it fails to predict the crystallization sequence inferred for lunar basalts owing to the low fO_2 of the system (Slater et al., 2003; Thompson et al., 2003). The mass-balance calculation aims to reproduce δ^{18}O and major-element variations between two melts: one relatively Mg-rich (starting melt) and one relatively Fe-rich (final melt). For a given starting melt, the oxide composition of the residual liquid can be approximated using a simple mass-balance calculation:

$$C_i = \left(C_{i,0} - \sum f_{\min} C_{i,\min}\right) \Big/ \left(1 - \sum f_{min}\right),$$

where C_i denotes the oxide wt% of the residual liquid, $C_{i,0}$ is the oxide wt% of the starting melt, min denotes the participating mineral phases, and $f_{\min}$ is the weight fraction of each mineral. We assume a constant mineral chemical composition in this calculation. Observed mineral phases (e.g., high-Ti from Rhodes et al., 1976; low-Ti from Rhodes and Hubbard, 1973) are used in this calculation. The final mineral assemblage is determined by varying the weight fractions of minerals ($f_{\min}$) until the calculated major-element oxide composition of the residual liquid matches the final melt. Based on these derived weight fractions of minerals, the δ^{18}O value of the residual liquid is calculated using the oxygen-fractionation factors between mineral phases assuming batch equilibrium crystallization. The oxygen-isotope fractionation between a melt and a solid of the same chemical composition is assumed to be zero (Eiler, 2001). The oxygen-fractionation factors for olivine–clinopyroxene ($\Delta^{18}O_{ol-cpx} \approx -0.5‰$) and olivine–plagioclase ($\Delta^{18}O_{ol-plag} \approx -0.9‰$) are calculated at 1100 °C using experimentally-derived expressions (Chiba et al., 1989; Clayton et al., 1989). The oxygen-fractionation factors for olivine–chromite ($\Delta^{18}O_{ol-crt} \approx 0.7‰$) and olivine–ilmenite ($\Delta^{18}O_{ol-ilm} \approx 0.5‰$) are calculated from quartz–chromite and quartz–ilmenite (Zheng, 1991) and from quartz–olivine (Chiba et al., 1989; Clayton et al., 1989). Oxygen-isotope fractionation factors between armalcolite ($(MgFe)Ti_2O_5$) and other minerals have not been experimentally determined. We estimate the value by considering armalcolite as a stoichiometric mixture of ilmenite ($FeTiO_3$), geikielite ($MgTiO_3$) and rutile (TiO_2), and using fractionations between ilmenite–quartz, geikielite–quartz, and rutile–quartz (Zheng, 1991). The calculated fractionation between chromite and armalcolite is $\Delta^{18}O_{crt-armal} \approx -0.5‰$. We use an equilibrium δ^{18}O value for lunar olivine of 5.15‰ based on the following evidence. Previous measurements on olivine separates reported that olivine in a high-Ti basalt (10020) has δ^{18}O of 5.14‰ (Onuma et al., 1970), and those

in low-Ti basalts (Apollo 12 and 15) range from 4.99‰ to 5.24‰ (Clayton et al., 1971, 1973). Spicuzza et al. (2007) estimated that olivine in equilibrium with low-Ti and high-Ti basalts would have a value of 5.15‰. For this model, mineral–mineral oxygen-isotope fractionation factors are assumed to be constant.

The mass-balance calculation is carried out using samples from the same subgroup of high-Ti basalts, which are thought to be related through fractional crystallization, (e.g., Shih et al., 1975; Rhodes et al., 1976; Neal et al., 1990; Snyder et al., 1990; Neal and Taylor, 1992; Jerde et al., 1994). Of all the high-Ti samples analyzed, Apollo 17 Type A basalts show the largest range in their major-element compositional variations, and are thus used for oxygen-isotope fractionation calculations. The most magnesian sample (70135, Mg# = 48, $\delta^{18}O = 5.59‰$) is used to represent the composition of the starting melt, and the least magnesian sample (75015, Mg# = 34, $\delta^{18}O = 5.66‰$) is used to represent the composition of the residual melt (Table 2). A total of ~31 wt% crystallization reproduces the major-element and $\delta^{18}O$ variations between the starting (70135) and the final melt (75015). The major-element and oxygen isotope ($\delta^{18}O$) compositions of the calculated final melt differ by less than 0.4 wt% and 0.06‰, respectively, relative to oxide contents and the measured oxygen isotope compositions for 75015 (Table 2 and Fig. 1). The fractionated mineral assemblage (Table 2) is similar to those derived by Rhodes et al. (1976). The calculated composition of the residual liquid is insensitive to small variations in weight fractions of silicates and ilmenite; a change of 0.01 in the weight fraction of minerals involved causes a change of ⩽0.4 wt% for major-element contents. However, changing the weight fraction of armalcolite by 0.01 will change SiO_2 and TiO_2 by ~1 wt%. The calculated $\delta^{18}O$ of the final melt is also insensitive to small variations in weight percentages of each mineral. Considering the combined uncertainty in the measured and modeled $\delta^{18}O$ values, the calculated $\delta^{18}O$ (5.72‰) is in reasonable agreement with the measured value of 75015 (5.66‰).

Similar calculations are conducted for low-Ti basalts. Table 3 shows the calculation for olivine-norm Apollo 15 low-Ti basalts. It is well established that low-Ti basalts were affected by removal of olivine ± pigeonite for samples with MgO < 12 wt% and by addition of olivine ± pigeonite for samples with MgO > 12 wt% (e.g., Rhodes and Hubbard, 1973; Rhodes et al., 1977). The systematic variation of $\delta^{18}O$ with major-element concentrations within individual subgroups of low-Ti basalts (Fig. 1) is consistent with these observations. Using Apollo 15 olivine-normative basalts as an example, and selecting 15016 (Mg# = 48, $\delta^{18}O = 5.62‰$) as the starting melt and 15556 (Mg# = 40, $\delta^{18}O = 5.72‰$) as the final melt, removing about 12 wt% olivine (Fo_{69}) and 0.5 wt% chromite produces a calculated melt of $\delta^{18}O = 5.69‰$, in excellent agreement with the measured value for 15557 (5.72‰). Perhaps more important than the fit for these two individual samples is the close

Table 2
Mass-balance model for crystal fractionation of high-Ti basalts.

Weight fraction (f)[a]	$\sum f = 0.311$								
	0.09 Ol[c]	0.003 Crt[c]	0.09 Arm[c]	0.115 Aug[c]	0.01 Plag[c]	0.003 Ilm[c]	Starting[b] 70135	Final Calculated	Final[b] 75015
SiO_2	36.7	0.06	0	47.7	47.5	0	38.0	41.5	41.9
TiO_2	0.11	3.39	73.7	3.09	0	54.0	13.5	9.18	9.13
Al_2O_3	0	12.1	1.60	4.01	33.4	0.04	7.92	10.0	9.98
Cr_2O_3	0.15	46.1	1.32	0.88	0	0.93	0.56	0.19	0.17
MgO	35.2	3.84	4.81	15.0	0.19	4.69	9.58	5.82	5.80
CaO	0.29	0.07	0.20	18.8	17.5	0.02	10.6	12.0	11.9
FeO	26.7	31.3	18.6	8.65	0.33	40.2	18.7	20.0	20.0
Na_2O	0	0	0	0.08	1.40	0	0.35	0.47	0.48
Total	99.2	96.9	100.3	98.2	100.4	99.9	99.2	99.3	99.4
$\delta^{18}O$[d] (‰)	5.15	4.43	*4.93*	5.64	6.04	4.65	5.59	5.72	5.66
Mg#	70		32	75.8			48.0	34.3	34.3

[a] Weight fraction (f) of each mineral phase that is removed, $\sum f$ is the total fraction of crystals removed.

[b] Sample (70135) is the only Type A sample with high Mg# (48) and high-TiO_2 (~13.5 wt%), and thus is used as the starting-melt composition. One of the lowest Mg# (34), Type A samples (75015) is selected as the final-melt composition after crystal–liquid fractionation.

[c] Mineral compositions are from Hill et al. (2006). Ol, olivine; Crt, chromite; Arm, armalcolite with a composition of $(Mg_{0.5}\ Fe_{0.5})Ti_2O_5$; Aug, augite; Pig, pigeonite; Plag, plagioclase; Ilm, ilmenite. Olivine and augite are the most Mg-rich compositions observed in 70135. Olivine is slightly more Fe-rich than the equilibrium value (Mg# = 74) using $K_{D,Fe-Mg}^{Ol-liq} = 0.32$ (Longhi et al., 1978) and augite is slightly more Mg-rich than the equilibrium value (Mg# = 74) with observed olivine using $K_{D,Fe-Mg}^{Ol-Px} = 1.0$ (Longhi and Pan, 1989). These changes could be due to Fe–Mg exchange of olivine and augite with each other and with melt.

[d] Equilibrium $\delta^{18}O$ of each mineral was derived from oxygen-fractionation factors for ol–plag and ol–pyroxene from Chiba et al. (1989). The oxygen-fractionation factor for ol–crt and ol–ilm are calculated from quartz–crt and quartz–ilm from Zheng (1991) and quartz–ol from Chiba et al. (1989) and Clayton et al. (1989). Oxygen-fractionation of armalcolite-melt has not been determined. We estimate the value by prorating fractionations assuming armalcolite is a mixture of ilmenite ($FeTiO_3$), geikielite ($MgTiO_3$) and TiO_2. Equilibrium $\delta^{18}O$ value of olivine (5.15‰) was estimated in Spicuzza et al. (2007), but is similar to measurements of olivine separates (Onuma et al., 1970; Clayton et al., 1971, 1973). The fractionation between a melt and a solid of the same composition is assumed to be 0 (Eiler, 2001).

Table 3
Mass-balance calculation for crystal fractionation of Apollo 15 olivine-normative basalts.

Weight fraction (f)	$\sum f = 0.125$				
	0.12	0.005	Starting	Final	
	Ol	Crt	15016	Calculated	15556
SiO_2	36.9	0.06	44.2	45.5	45.6
TiO_2	0.02	2.83	2.33	2.64	2.60
Al_2O_3	0	12.3	8.48	9.62	9.47
Cr_2O_3	0.41	50.8	0.82	0.59	0.67
MgO	28.1	27.3	22.3	21.5	21.7
CaO	34.1	6.56	11.2	8.09	8.14
FeO	0.30	0.07	9.23	10.5	10.6
Na_2O	0	0	0.25	0.29	0.27
Total	99.8	99.7	98.8	98.7	99.1
$\delta^{18}O$ (‰)	5.15	4.43	5.62	5.69	5.72
Mg#	69	66	47.5	40.4	40.3

fit between the slope of the line generated by modeling compared to a best fit line through all of the low-Ti basalt data (Fig. 2). Overall, the above simplified calculation demonstrates that the crystal fractionation is capable generating the observed $\delta^{18}O$ changes with major-element composition in mare basalts.

4.2. Iron isotope variations in low-Ti and high-Ti groups

It is shown above that oxygen isotope variations in mare basalts can be successfully modeled by crystal fractionation. In contrast, iron isotope compositions are not correlated with the index of fractionation (Mg#) in either low-Ti or high-Ti basalts (Fig. 5c), suggesting that near-surface crystal fractionation did not impart significant iron isotopic fractionation. This observation differs from iron isotopic fractionation measured from Kilauea Iki lava lake, Hawai'i, where it was shown that residual liquids displayed enrichments up to 0.2‰ in $\delta^{56}Fe$ relative to early (olivine) cumulates (Teng et al., 2008). The different behavior of iron isotopes during crystal fractionation of lunar mare basalts may reflect negligible Fe isotopic fractionation under extremely reducing conditions relevant to lunar basalt petrogenesis (Dauphas et al., 2009a). The lower susceptibility of iron isotopic fractionation during low-pressure crystal fractionation of lunar mare basalts therefore makes iron isotopes potentially good tracers of lunar mantle compositions.

The overall heavy iron isotopic composition of high-Ti mare basalts relative to low-Ti basalts likely reflects mineralogical controls within lunar mantle source regions. Although there is a linear correlation of $\delta^{56}Fe$ and TiO_2, the nearly parallel trends in $\delta^{56}Fe$ versus Mg# and $\delta^{56}Fe$ versus Al_2O_3 are inconsistent with a magma mixing origin for the low-Ti and high-Ti groups (Fig. 5b and c). On the basis of the correlation between $\delta^{56}Fe$ and $\delta^{18}O$ in the least differentiated low-Ti and high-Ti basalts, causes of the $\delta^{18}O$ variations between mare basalts can be used as a reference to help interpret $\delta^{56}Fe$ variations because there are limited studies of iron isotopic fractionation between minerals and melt. It is generally accepted that oxygen isotope differences between low-Ti and high-Ti groups reflect variable proportions of ilmenite within their mantle sources (e.g., Spicuzza et al., 2007). As ilmenite has lower $\delta^{18}O$ than silicates (Section 4.1), high-Ti melt from ilmenite-rich mantle rocks will contain lower $\delta^{18}O$ than low-Ti melt from ilmenite-poor rocks. The negative correlation between oxygen and iron-isotope ratios (Fig. 6) indicates that ilmenite contains higher $\delta^{56}Fe$ than silicates. Indeed, the heavier $\delta^{56}Fe$ of ilmenite versus silicates (clinopyroxene, pigeonite) has been demonstrated in a recent study of iron isotopic variations in lunar basalt mineral separates (Craddock et al., 2010).

4.3. Oxygen and iron isotope compositions of mare basalt mantle sources

It has long been realized that low-Ti and high-Ti basalts are derived from different mantle sources (e.g., Taylor, 1975; Walker et al., 1975; Shearer et al., 2006). Low-Ti basalts are interpreted as partial melt derivatives from olivine + orthopyroxene dominated mantle sources, whereas high-Ti basalts are thought to be derived from ilmenite-rich source regions generated either by cumulate sinking and remelting (e.g., Spera, 1992; Hess and Parmentier, 1995), or from assimilation of ilmenite-rich cumulates by very-low-Ti melts during magma ascent (e.g., Hubbard and Minear, 1975; Wagner and Grove, 1997; Thacker et al., 2009). The parallel trends between low-Ti and high-Ti basalts in $\delta^{18}O$–Al_2O_3, $\delta^{56}Fe$–Al_2O_3, $\delta^{18}O$–Mg#, and $\delta^{56}Fe$–Mg# plots (Figs. 1b and c, and 5b and c) are inconsistent with simple mixing of different basalt mantle sources, or with the assimilation of ilmenite-rich cumulates by low-Ti melts. In addition, low-Ti and high-Ti basalts follow different trends in initial $^{143}Nd/^{144}Nd$ and $^{176}Hf/^{177}Hf$ space (e.g., Unruh et al., 1984; Beard et al, 1998), implying that low-Ti and high-Ti basalts were derived from mantle sources with distinct mineral assemblages. Hypotheses of different degrees of partial melting of the same source rock are not supported by highly-siderophile-element abundances in mare basalts (e.g., Day et al., 2007). In addition, it is extremely difficult to melt the right proportion of minerals in ilmenite-rich cumulates to generate the estimated melt compositions for high-Ti mare basalts (Van Orman

and Grove, 2000). The popular model for mare basalt genesis is cumulate sinking and remelting, which suggests that ilmenite-rich cumulates formed after ~95% crystallization of the lunar magma ocean, and were subsequently mixed into the deeper mantle owing to density instability (Spera, 1992; Hess and Parmentier, 1995).

The $\delta^{18}O$ value of mantle sources for low-Ti and high-Ti melts can be estimated using the proposed source mineralogy in Snyder and Taylor (1993) and Snyder et al. (1992), respectively. The mantle source mineralogy for high-Ti and very-low-Ti basalts was estimated in these studies so that calculated melts from these mantle sources had major- and trace-element abundances very similar to those of low-Ti and high-Ti mare basalts (Snyder et al., 1992; Snyder and Taylor, 1993). Snyder et al. (1992) suggested that the source for high-Ti basalts consists of 46% pigeonite, 43% olivine, 7% clinopyroxene, 3% ilmenite and 1% plagioclase (or 1–2% trapped KREEPy liquid). The estimate for very-low-Ti basalt (60% orthopyroxene and 40% olivine) by Snyder and Taylor (1993) is used to approximate the source for low-Ti basalts. The high-temperature oxygen-isotope equilibrium of the lunar mantle enables the use of equilibrium values of minerals for the estimate. Using oxygen-isotope fractionation factors between minerals described above, mantle olivine of 5.15‰, and a 0.4‰ oxygen-isotope fractionation factor between orthopyroxene and clinopyroxene (Chacko et al., 2001), the calculated bulk $\delta^{18}O$ values of high-Ti and very-low-Ti sources are 5.30‰ and 5.57‰ at 1300 °C, respectively. This calculation was conducted for a very-low-Ti source. Low-Ti source may have more pigeonite. Replacing some of the orthopyroxene with 30 wt% pigeonite decreases the estimated $\delta^{18}O$ of the low-Ti source by 0.12‰. Considering the uncertainty in mineralogy of both source rocks and the associated equilibrium oxygen isotope value, we suggest the 2σ uncertainty of source $\delta^{18}O$ values to be ±0.2‰.

Iron isotope fractionation factors between minerals (oxides and silicates) relevant to lunar petrology have not been experimentally determined. Therefore, we estimate the iron isotope composition of mantle rocks from that of mare basalts after accounting for potential isotopic fractionation during crystal fractionation and partial melting. We have shown above that crystal fractionation has a negligible effect on the iron isotope compositions of mare basalts (Fig. 5). The iron isotopic fractionation associated with partial mantle melting on the Moon is less certain. A small, but significant, partial melting effect on iron isotopes has been demonstrated for terrestrial mid-oceanic ridge basalts (MORB) and oceanic island basalts (OIB) (e.g., Williams et al., 2005; Weyer and Ionov, 2007; Dauphas et al., 2009a). Modern MORB and OIB have systematically heavier iron-isotope ratios by 0.05–0.1‰ relative to primitive mantle peridotites and high-degree partial melts (Weyer and Ionov, 2007; Dauphas et al., 2009a, 2010), which have compositions more similar to chondrites and basalts from Vesta and Mars (Poitrasson et al., 2004, 2005; Weyer et al., 2005; Anand et al., 2006; Schoenberg and von Blanckenburg, 2006; Dauphas et al., 2009a; Craddock and Dauphas, 2010). These studies imply that the iron isotope compositions of MORB do not directly reflect that of the terrestrial upper mantle (Weyer and Ionov, 2007; Dauphas et al., 2009a, 2010). Were iron isotopes in mare basalts also fractionated during partial melting on the Moon? A partial melting model developed by Dauphas et al. (2009a) proposes that heavy iron isotope compositions of MORB and OIB reflect equilibrium isotopic fractionation between Fe^{3+} and Fe^{2+} ($\Delta^{56}Fe_{Fe(III)-Fe(II)} \sim +0.3‰$; cf., Polyakov and Mineev, 2000; Schuessler et al., 2007; Schoenberg et al., 2009) during partial melting and preferential extraction of Fe^{3+} into melt. The intrinsic oxygen fugacity of lunar mare basalts is IW-0.2 to IW-1 (Sato et al., 1973; Sato, 1976), suggesting that Fe^{3+} is essentially absent on the Moon and Fe^0 is stable in the lunar interior. Applying the model of Dauphas et al. (2009a) to the Moon suggests that partial melting of the lunar mantle might yield negligible iron isotopic fractionation. However, possible iron isotopic fractionation during partial melting under extremely reduced conditions (in the presence of both Fe^{2+} and Fe^0) must also be considered. Based on experimental and theoretical estimates for core formation, equilibrium iron isotope fractionation between iron metal and silicate appears to be small at low pressures and high temperatures (e.g., $\Delta^{56}Fe_{silicate-metal} \approx -0.03‰$ at 1500 °C and 0 GPa, Roskosz et al., 2006; Polyakov et al., 2007; Polyakov, 2009). These data imply that partial melting of iron metal-bearing rocks at the IW buffer or lower, high temperatures (1100–1200 °C) and low pressures should also yield negligible iron isotopic fractionation. More involved models of iron isotope fractionation during partial melting of lunar mantle sources with exotic phases including iron metal, ilmenite and/or armalcolite are required to fully assess this hypothesis. However, as a first estimate, we suggest that the average $\delta^{56}Fe$ values of low-Ti basalts ($0.073 \pm 0.018‰$, $n = 8$) and high-Ti basalts ($0.191 \pm 0.020‰$, $n = 7$) may directly record that of their parent mantle sources.

4.4. Oxygen and iron isotope composition of the lunar upper mantle

Low-Ti and high-Ti basalts are melts derived from the lunar upper mantle following removal of the anorthite-rich lunar crust, as demonstrated by their ubiquitous negative Eu anomaly (e.g., Taylor, 1975). Experiments of multiple-saturation points predict a melting depth of 200–400 km or deeper for the generation of low-Ti and high-Ti melts (see Longhi, 1992). These experimental results correspond to the estimated transition depth (~500 km) from the upper to lower lunar mantle based on seismic velocity modeling (Nakamura, 1983). Therefore, the $\delta^{18}O$ and $\delta^{56}Fe$ of the lunar upper mantle can be estimated using the mantle source values for low-Ti and high-Ti mare basalts (Section 4.3).

Two lines of evidence argue that the lunar upper mantle is likely composed predominantly of the mineral assemblage olivine + pyroxene that melted to form the low-Ti basalts. First, modeling of magma ocean crystallization by Snyder et al. (1992) suggests that >78% of the lunar magma ocean crystallized to form olivine and orthopyroxene, whereas ilmenite-rich cumulates formed only after 95% crystallization. Second, Clementine remote sensing data for

lunar surface TiO_2 abundances in lunar mare region show that basalts with low-Ti affinities make up ~90% of all mare basalts exposed on the lunar surface (Giguere et al., 2000). Thus, it is likely that any estimate of the lunar upper mantle would be weighted towards low-Ti basalt sources (e.g., Spicuzza et al., 2007). For the purpose of these calculations we assume that lunar upper mantle is composed of ~90 wt% low-Ti and 10 wt% high-Ti cumulate source, acknowledging some degree of uncertainty in this estimate. Using our estimate for the isotopic composition of low-Ti and high-Ti basalt mantle sources (Section 4.3), the oxygen and iron isotope compositions of bulk lunar upper mantle calculated accordingly are $\delta^{18}O = 5.5‰$ and $\delta^{56}Fe = 0.085‰$. The 2σ uncertainties on these estimates are $\pm 0.2‰$ for $\delta^{18}O$ and $\pm 0.04‰$ for $\delta^{56}Fe$, taking into account uncertainties in the bulk lunar upper mantle composition (±10 wt% uncertainty in the relative fractions of different sources in the mantle) and uncertainties in the calculated average oxygen and iron isotope compositions of low-Ti and high-Ti basalts (Section 4.3).

The $\delta^{18}O$ value of the lunar upper mantle is the same as that estimated composition for peridotites in the terrestrial upper mantle ($+5.5 \pm 0.2‰$, Eiler, 2001). To a first order approximation, the similarity between $\delta^{18}O$ estimates for the lunar mantle and terrestrial mantle implies that fractionation of O by water-driven processes at the Earth's surface has not fractionated $^{18}O/^{16}O$ significantly between the bulk terrestrial crust and mantle reservoirs, to be detectable at the current levels of precision (Valley et al., 2005).

The inferred $\delta^{56}Fe$ value of the lunar upper mantle ($+0.085 \pm 0.030‰$) overlaps with recent estimates for that of the bulk-silicate Earth ($+0.02 \pm 0.03‰$, Weyer and Ionov, 2007; $+0.044 \pm 0.030‰$, Dauphas et al., 2010), but may be heavier than that of primitive chondrites (~0‰, Schoenberg and von Blanckenburg, 2006; Dauphas et al., 2009b; Craddock and Dauphas, 2010) and basalts of Mars and Vesta ($+0.011 \pm 0.010‰$, Poitrasson et al., 2004; Weyer et al., 2005; Anand et al., 2006; Schoenberg and von Blanckenburg, 2006). If correct, a number of processes may have produced a lunar upper mantle with a non-chondritic iron isotopic composition. Poitrasson et al. (2004) previously suggested that preferential loss (evaporation) of isotopically light iron during the giant impact produced an Earth–Moon system enriched in the heavy isotopes of iron. According to this hypothesis, the composition of both the lunar mantle and the bulk-silicate Earth should be non-chondritic. The latter, however, is not clearly supported by observations that terrestrial mantle rocks and high-degree partial melts have an iron isotopic composition the same as chondrites within uncertainties (Weyer and Ionov, 2007; Dauphas et al., 2010). Alternatively, large-scale planetary differentiation (e.g., core formation) may have formed a silicate mantle with non-chondritic composition if there was iron isotopic fractionation between iron metal and silicate. Experimental and theoretical studies of high temperature (~1500 °C) equilibrium iron isotope fractionation between metal and silicate yield a range of results from small fractionations ($\Delta^{56}Fe_{metal-silicate} < 0.1‰$) at low pressures (0 GPa) to larger, negative fractionations (~−0.3‰) at high pressure (130 GPa) (e.g., Roskosz et al., 2006; Polyakov, 2009). Conditions of planetary differentiation on the Moon are uncertain, but may have occurred at relatively low pressure (the pressure at the center of the Moon is ~4 GPa, e.g., Wieczorek et al., 2006) implying negligible iron isotopic fractionation during lunar core formation. Finally, partial melting under extremely reduced conditions (in the presence of both Fe^{2+} and Fe^0) might also produce iron isotopic fractionation observed in lunar basalts. There are, however, no independent experimental or theoretical constraints on this process. Further studies are necessary to constrain the magnitude of equilibrium iron isotopic fractionation between possible iron oxidation states and iron coordination in minerals and melt relevant to lunar basalt petrogenesis. Given these uncertainties, it is not yet clear that the lunar upper mantle estimate of $\delta^{56}Fe$ is the same as the bulk Moon and whether the bulk Moon has a chondritic or non-chondritic iron isotopic composition.

5. SUMMARY

We report combined oxygen and iron isotope compositions for mare basalts. Combined with oxygen isotope data from the same laboratory (Spicuzza et al., 2007), this internally-consistent dataset for oxygen isotopes now encompasses a suite of mare basalts with a wide range of major-element compositions from $TiO_2 = 1.7$ to 13.5 wt% and Mg# = 34 to 55. An important aspect of this study is the correlation of oxygen isotope composition with the index of fractionation (e.g., Mg#). This composition-dependent variation of $\delta^{18}O$ is distinct in high-Ti basalts with an increase in $\delta^{18}O$ of ~0.3‰ between basalts with Mg# = 53 (least differentiated) and Mg# = 34 (more differentiated). Variations of $\delta^{18}O$ within low-Ti basalts are much smaller in magnitude (~0.15‰) but still resolvable using high-precision measurements of numerous samples across a wide compositional spectrum (Mg# = 55–38). The coupling of $\delta^{18}O$ with major-element compositions of both low-Ti and high-Ti basalts is consistent with isotopic fractionation caused by near-surface crystal fractionation and matches well with model calculations.

High-precision iron isotope analyses were conducted on 15 mare basalts. The $\delta^{56}Fe$ and $\delta^{57}Fe$ values show mass-dependent fractionation similar to terrestrial rocks. Low-Ti basalts contain lower $\delta^{56}Fe$ values than high-Ti basalts. Within each group, $\delta^{56}Fe$ values are decoupled from major-element compositions, reflecting insignificant control from crystal fractionation.

The oxygen and iron isotope compositions are remarkably different between low-Ti and high-Ti basalts. Low-Ti and high-Ti basalt compositions do not follow simple binary mixing trends with respect to $\delta^{18}O$ ratios, $\delta^{56}Fe$ ratios, and major- and trace-element abundances. The difference in $\delta^{18}O$ and $\delta^{56}Fe$ between low-Ti and high-Ti basalts is likely due to modal mineralogical differences within and between their mantle sources. Using previously proposed mantle mineralogy, the oxygen and iron isotope compositions of the mantle sources are inferred to be $5.5 \pm 0.2‰$ and $0.085 \pm 0.040‰$, respectively. Our estimates are identical to estimates for the terrestrial upper mantle values.

ACKNOWLEDGMENTS

We thank the CAPTEM team and particularly the Lunar Sample Curatorial staff for their co-operation in making this study possible. We thank three anonymous reviewers for their critical comments on versions of this manuscript and C. Koeberl for editorial handling. Portions of this study were supported by the NASA Cosmochemistry Program NNG05GG03G (L.A.T.) and NNX09AG59G (N.D.), the LASER Program NNX08AY83G (J.W.V.), and the NASA Astrobiology Institute, and a Packard fellowship to N.D.

APPENDIX A. SUPPLEMENTARY DATA

Supplementary data associated with this article can be found, in the online version, at doi:10.1016/j.gca.2010.08.008.

REFERENCES

Albarède F. and Beard B. (2004) Analytical methods for non-traditional isotopes. *Rev. Mineral. Geochem.* **55**, 113–152.

Anand M., Russell S. S., Blackhurst R. L. and Grady M. M. (2006) Searching for signatures of life on Mars: an Fe-isotope perspective. *Philos. Trans. R. Soc. B* **361**, 1715–1720.

Beard B. L., Taylor L. A., Scherer E. E., Johnson C. M. and Snyder G. A. (1998) The source region and melting mineralogy of high-titanium and low-titanium lunar basalts deduced from Lu–Hf isotope data. *Geochim. Cosmochim. Acta* **62**, 525–544.

Beaty D. W. and Albee A. L. (1978) Comparative petrology and possible petrogenetic relations among the Apollo 11 basalts. *Proc. 9th Lunar Planet. Sci.*, 359–463.

Belshaw N. S., Zhu X. K., Guo Y. and O'Nions R. K. (2000) High precision measurement of iron isotopes by plasma source mass spectrometry. *Int. J. Mass Spectrom.* **197**, 191–195.

Cameron A. G. W. (1997) The origin of the moon and the single impact hypothesis. V. *Icarus* **126**, 126–137.

Canup R. M. and Asphaug E. (2001) Origin of the Moon in a giant impact near the end of the Earth's formation. *Nature* **412**, 708–712.

Chacko T., Cole D. R. and Horita J. (2001) Equilibrium oxygen, hydrogen and carbon isotope fractionation factors applicable to geologic systems. *Rev. Mineral. Geochem.* **43**, 1–81.

Chiba H., Chacko T., Clayton R. N. and Goldsmith J. R. (1989) Oxygen isotope fractionations involving diopside, forsterite, magnetite, and calcite: application to geothermometry. *Geochim. Cosmochim. Acta* **53**, 2985–2995.

Clayton R. N., Goldsmith J. R. and Mayeda T. K. (1989) Oxygen isotope fractionation in quartz, albite, anorthite and calcite. *Geochim. Cosmochim. Acta* **53**, 725–733.

Clayton R. N., Grossman L. and Mayeda T. K. (1973) Component of primitive nuclear composition in carbonaceous meteorites. *Science* **182**, 485–488.

Clayton R. N., Hurd J. M. and Mayeda T. K. (1971) Oxygen isotopic compositions of Apollo 15, 16, and 17 samples, and their bearing on lunar origin and petrogenesis. *Proc. Lunar Sci. Conf. 4th*, 1417–1420.

Craddock P. R. and Dauphas N. (2010) Iron isotopic compositions of reference materials, geostandards and chondrites. *Geostand. Geoanal. Res.* (in press).

Craddock P. R., Dauphas N., and Clayton R. N. (2010) Mineralogical control on iron isotopic fractionation during lunar differentiation and magmatism. *Lunar Planet. Sci. Conf. 41st*, #1230.

Dauphas N., Craddock P. R., Asimow P. D., Bennett V. C., Nutman A. P. and Ohnenstetter D. (2009a) Iron isotopes may reveal the redox conditions of mantle melting from Archean to present. *Earth Planet. Sci. Lett.* **288**, 255–267.

Dauphas N., Janney P. E., Mendybaev R. A., Wadhwa M., Richter F. M., Davis A. M., van Zuilen M., Hines R. and Foley C. N. (2004) Chromatographic separation and multicollection-ICPMS analysis of iron. Investigating mass-dependent and -independent isotope effects. *Anal. Chem.* **76**, 5855–5863.

Dauphas N., Pourmand A. and Teng F.-Z. (2009b) Routine isotopic analysis of iron by HR-MC-ICPMS: how precise and how accurate? *Chem. Geol.* **267**, 157–184.

Dauphas N., Teng F.-Z. and Arndt N. T. (2010) Magnesium and iron isotopes in 2.7 Ga Alexo komatiites: mantle signatures, no evidence for Soret diffusion, and identification of diffusive transport in zoned olivine. *Geochim. Cosmochim. Acta* **74**, 3274–3291.

Dauphas N. and Rouxel O. (2006) Mass spectrometry and natural variations of iron isotopes. *Mass Spectrom. Rev.* **25**, 515–550, Erratum 25, 831–832..

Day J. M. D., Pearson D. G. and Taylor L. A. (2007) Highly siderophile element constraints on accretion and differentiation of the Earth–Moon system. *Science* **315**, 217–219.

Day J. M. D., Taylor L. A., Floss C., Patchen A. D., Schnare D. W. and Pearson D. G. (2006) Comparative petrology, geochemistry, and petrogenesis of evolved, low-Ti lunar mare basalt meteorites from the LaPaz Icefield, Antarctica. *Geochim. Cosmochim. Acta* **70**, 1581–1600.

Eiler J. M. (2001) Oxygen isotope variations of basaltic lavas and upper mantle rocks. *Rev. Mineral. Geochem.* **43**, 319–364.

Eiler J. M., Schiano P., Kitchen N. and Stolper E. M. (2000) Oxygen-isotope evidence for recycled crust in the sources of mid-ocean-ridge basalts. *Nature* **403**, 530–534.

Georg R. B., Halliday A. N., Schauble E. A. and Reynolds B. C. (2007) Silicon in the Earth's core. *Nature* **447**, 1102–1106.

Giguere T., Taylor G. J., Hawke B. R. and Lucey P. G. (2000) The titanium contents of lunar mare basalts. *Meteorit. Planet. Sci.* **35**, 193–200.

Ghiorso M. S. and Sack R. O. (1995) Chemical mass transfer in magmatic processes IV. A revised and internally consistent thermodynamic model for the interpolation and extrapolation of liquid–solid equilibria in magmatic systems at elevated temperatures and pressures. *Contrib. Mineral. Petrol.* **119**, 197–212.

Hallis L. J., Greenwood R. C., Anand M., Russell S. S., Miller M. F., and Franchi I. A. (2009) Oxygen isotopic composition of mare-basalts: magma ocean differentiation and source heterogeneity. In *72nd Annual Meteoritical Society Meeting*, #5314.

Hess P. C. and Parmentier E. M. (1995) A model for the thermal and chemical evolution of the Moon's interior: implications for the onset of mare volcanism. *Earth Planet. Sci. Lett.* **134**, 501–514.

Hill E., Day J. M. D., Davidson J., and Taylor L. A. (2006) Petrogenesis of Apollo 17 mare basalts-revisited. *Lunar Planet. Sci. Conf. 37*th, #2067.

Hubbard N. J. and Minear J. W. (1975) A physical and chemical model of early lunar history. *Proc. 6th Lunar Sci. Conf.*, 1057–1085.

Jerde E. A., Snyder G. A., Taylor L. A., Liu Y. G. and Schmitt R. A. (1994) The origin and evolution of lunar high-Ti basalts: periodic melting of a single-source at mare tranquillitatis. *Geochim. Cosmochim. Acta* **58**, 515–527.

Longhi J., Walker D. and Hays J. F. (1978) The distribution of Fe and Mg between olivine and lunar basaltic liquids. *Geochim. Cosmochim. Acta* **42**, 1545–1558.

Longhi J. (1992) Experimental petrology and petrogenesis of mare volcanics. *Geochim. Cosmochim. Acta* **56**, 2235–2251.

Longhi J. and Pan V. (1989) The parent magmas of the SNC meteorites. *Proc. Lunar Planet. Sci. Conf. 19th*, 451–464.

Malinovsky D., Stenberg A., Rodushkin I., Andren H., Ingri J., Öhlander B. and Baxter D. C. (2003) Performance of high resolution MC-ICP-MS for Fe isotope ratio measurements in sedimentary geological materials. *J. Anal. At. Spectrom.* **18**, 687–695.

Melosh H. J. (2009) An isotopic crisis for the giant impact origin of the Moon? In *72nd Annual Meteoritical Society Meeting*, #5104.

Meyer C. (2004–2008) Lunar sample compendium. Available from: <http://www-curator.jsc.nasa.gov/lunar/compendium.cfm>.

Nakamura Y. (1983) Seismic velocity structure of the lunar mantle. *J. Geophys. Res.* **88**, 677–686.

Neal C. R. (2001) Interior of the Moon: the presence of garnet in the primitive deep lunar mantle. *J. Geophys. Res.-Planets* **106**, 27865–27885.

Neal C. R. (2008) Mare basalt database. Available from: <http://www.nd.edu/~cneal/Lunar-L/>.

Neal C. R. and Taylor L. A. (1992) Petrogenesis of mare basalts – a record of lunar volcanism. *Geochim. Cosmochim. Acta* **56**, 2177–2211.

Neal C. R., Taylor L. A., Hughes S. S. and Schmitt R. A. (1990) The Significance of fractional crystallization in the petrogenesis of Apollo-17 Type-A and Type-B high-Ti basalts. *Geochim. Cosmochim. Acta* **54**, 1817–1833.

Onuma N., Clayton R. N., and Mayeda T. K. (1970) Apollo 11 rocks: oxygen isotope fractionation between minerals, and an estimate of the temperature of formation. *Proceedings of the Apollo 11 Lunar Science Conference* 2, pp. 1429–1434.

Pahlevan K. and Stevenson D. J. (2007) Equilibration in the aftermath of the lunar-forming giant impact. *Earth Planet. Sci. Lett.* **262**, 438–449.

Papike J. J., Ryder G. and Shearer C. K. (1998) Lunar samples. *Rev. Mineral.* **36**, E1–E234.

Poitrasson F., Halliday A. N., Lee D. C., Levasseur S. and Teutsch N. (2004) Iron isotope differences between Earth, Moon, Mars and Vesta as possible records of contrasted accretion mechanisms. *Earth Planet. Sci. Lett.* **223**, 253–266.

Poitrasson F., Levasseur S. and Teutsch N. (2005) Significance of iron isotope mineral fractionation in pallasites and iron meteorites for the core–mantle differentiation of terrestrial planets. *Earth Planet. Sci. Lett.* **234**, 151–164.

Polyakov V. B. (2009) Equilibrium iron isotope fractionation at core–mantle boundary conditions. *Science* **323**, 912–914.

Polyakov V. B. and Mineev S. D. (2000) The use of Mössbauer spectroscopy in stable isotope geochemistry. *Geochim. Cosmochim. Acta* **64**, 849–865.

Polyakov V. B., Clayton R. N., Horita J. and Mineev S. D. (2007) Equilibrium iron isotope fractionation factors of minerals: reevaluation from the data of nuclear inelastic resonant X-ray scattering and Mössbauer spectroscopy. *Geochim. Cosmochim. Acta* **71**, 3833–3846.

Rhodes J. M., Hubbard N. J., Wiesmann H., Rodgers K. V., Brannon J. C. and Bansal B. M. (1976) Chemistry, classification, and petrogenesis of Apollo 17 mare basalts. *Proc. Lunar Planet. Sci.* **7**, 1467–1489.

Rhodes J. M. and Blanchard D. P. (1980) Chemistry of Apollo 11 low-K mare basalts. *Proc. Lunar Planet. Sci.* **11**, 49–66.

Rhodes J. M. and Hubbard N. J. (1973) Chemistry, classification and petrogenesis of Apollo 15 mare basalts. *Proc. Lunar Planet. Sci.* **4**, 1127–1148.

Rhodes J. M., Blanchard D. P., Dungan M. A., Brannon J. C. and Rodgers K. V. (1977) Chemistry of Apollo 12 mare basalts: magma types and fractionation processes. *Proc. Lunar Planet. Sci.* **8**, 1305–1338.

Roskosz M., Luais B., Watson H. C., Toplis M. J., Alexander C. M. O. D. and Mysen B. O. (2006) Experimental quantification of the fractionation of Fe isotopes during metal segregation from a silicate melt. *Earth Planet. Sci. Lett.* **248**, 851–867.

Sato M. (1976) Oxygen fugacity and other thermochemical parameters of Apollo 17 high-Ti basalts and their implications on the reduction mechanism. *Proc. Lunar Planet. Sci.* **7**, 1323–1344.

Sato M., Hicklinc N. L. and Mclane J. E. (1973) Oxygen fugacity of Apollo 12. 14 and 15 lunar samples and reduced state of lunar magmas. *Proc. Lunar Sci. Conf.* **4**, 1061–1079.

Schnare D. W., Day J. M. D., Norman M. D., Liu Y. and Taylor L. A. (2008) A laser-ablation ICP-MS study of Apollo 15 low-titanium olivine-normative and quartz-normative mare basalts. *Geochim. Cosmochim. Acta* **72**, 2556–2572.

Schoenberg R. and von Blanckenburg F. (2006) Modes of planetary-scale Fe isotope fractionation. *Earth Planet. Sci. Lett.* **252**, 342–359.

Schoenberg R., Marks M. A. W., Schuessler J. A., von Blanckenburg F. and Markl G. (2009) Fe isotope systematics of coexisting amphibole and pyroxene in the alkaline igneous rock suite of the Ilímaussaq complex, South Greenland. *Chem. Geol.* **258**, 65–77.

Schuessler J. A., Schoenberg R., Behrens H. and Blanckenburg F. V. (2007) The experimental calibration of the iron isotope fractionation factor between pyrrhotite and peralkaline rhyolitic melt. *Geochim. Cosmochim. Acta* **71**, 417–433.

Shearer C. K., Hess P. C., Wieczorek M. A., Pritchard M. E., Parmentier E. M., Borg L. E., Longhi J., Elkins-Tanton L. T., Neal C. R., Antonenko I., Canup R. M., Halliday A. N., Grove T. L., Hager B. H., Lee D.-C. and Wiechert U. (2006) Thermal and magmatic evolution of the Moon. *Rev. Mineral. Geochem.* **60**, 365–518.

Shih C. Y., Haskin L. A., Wiesmann H., Bansal B. and Brannon J. C. (1975) On the origin of high-Ti mare basalts. *Proc. Lunar Planet. Sci. 6th*, 1255–1285.

Simon J. I. and DePaolo D. J. (2010) Stable calcium isotopic composition of meteorites and rocky planets. *Earth Planet. Sci. Lett.* **289**, 457–466.

Slater V. P., Thompson C. K., Nettles J., Milam K., Stockstill K. R., Cahill J., Anand M., and Taylor L. A. (2003) An evaluation of the igneous crystallization programs – MELTS, MAGPOX, and COMAGMAT part II: importance of magmatic f_{O2}. *Lunar Planet. Sci. Conf. 34th,* #1896.

Snyder G. A., Taylor L. A., and Neal C. R. (1990) The sources of mare basalts: a model involving lunar magma ocean crystallization, plagioclase floatation, and trapped instantaneous residual liquid. In *Workshop on Mare Basalt Petrogenesis*. Lunar and Planetary Institute, Houston, pp. 45–46 (abstr.).

Snyder G. A., Taylor L. A. and Neal C. R. (1992) A chemical-model for generating the sources of mare basalts: combined equilibrium and fractional crystallization of the lunar magmasphere. *Geochim. Cosmochim. Acta* **56**, 3809–3823.

Snyder G. A., and Taylor L. A. (1993) Constraints on the genesis and evolution of the Moon's magma ocean and derivative cumulate sources as supported by lunar meteorites. In *Proceedings of NIPR Symposium on Antarctic Meteorites*, vol. 6, pp. 246–267.

Spera F. J. (1992) Lunar magma transport phenomena. *Geochim. Cosmochim. Acta* **56**, 2253–2265.

Spicuzza M. J., Day J. M. D., Taylor L. A. and Valley J. W. (2007) Oxygen isotope constraints on the origin and differentiation of the Moon. *Earth Planet. Sci. Lett.* **253**, 254–265.

Spicuzza M. J., Valley J. W., and McConnell V. S. (1998) Oxygen isotope analysis of whole rock via laser fluorination: an air-lock approach. *GSA Abstracts with Programs* 30, A80.

Taylor S. R. (1975) *Lunar Science: A Post-Apollo View*. Pergamon Press, 372pp.

Taylor J. G., Warren P. H., Ryder G., Delano J., Pieters C. and Lofgren G. (1991) Lunar rocks. In *Lunar Sourcebook: A User's Guide to the Moon* (eds. G. H. Heiken, D. T. Vaniman and B. M. French). Cambridge University Press.

Taylor P. D. P., Maeck R. and De Bièvre P. (1992) Determination of the absolute isotopic composition and atomic weight of a reference sample of natural iron. *Int. J. Mass Spectrom. Ion Processes* **121**, 111–125.

Teng F.-Z., Dauphas N. and Helz R. T. (2008) Iron isotope fractionation during magmatic differentiation in Kilauea Iki lava lake. *Science* **320**, 1620–1622.

Teng F.-Z., Li W.-Y., Ke S., Marty B., Dauphas N., Huang S., Wu F.-Y. and Pourmand A. (2010a) Magnesium isotopic composition of the Earth and chondrites. *Geochim. Cosmochim. Acta* **74**, 4150–4166.

Thacker C., Liang Y., Peng Q. and Hess P. (2009) The stability and major element partitioning of ilmenite and armalcolite during lunar cumulate mantle overturn. *Geochim. Cosmochim. Acta* **73**, 820–836.

Thompson C. K., Slater V. P., Stockstill K. R., Anand M., Nettles J., Milam K., Cahill J., and Taylor L. A. (2003) An evaluation of the igneous crystallization programs – MELTS, MAGPOX, and COMAGMAT part I: does one size fit all? *Lunar Planet. Sci. Conf. 34th*, #1881.

Unruh D. M., Stille P., Patchett P. J. and Tatsumoto M. (1984) Lu–Hf and Sm–Nd evolution in lunar mare basalts. *J. Geophys. Res.* **89**, B459–B477.

Valley J. W., Kitchen N. E., Kohn M. J., Niendorf C. R. and Spicuzza M. J. (1995) UWG-2, a garnet standard for oxygen isotope ratio: strategies for high precision and accuracy with laser heating. *Geochim. Cosmochim. Acta* **59**, 5223–5231.

Valley J. W., Lackey J. S., Cavosie A. J., Clechenko C. C., Spicuzza M. J., Basei M. A. S., Bindeman I. N., Ferreira V. P., Sial A. N., King E. M., Peck W. H., Sinha A. K. and Wei C. S. (2005) 4.4 billion years of crustal maturation: oxygen isotope ratios of magmatic zircon. *Contrib. Mineral. Petrol.* **150**, 561–580.

Van Orman J. A. and Grove T. L. (2000) Origin of lunar high-titanium ultramafic glasses: constraints from phase relations and dissolution kinetics of clinopyroxene–ilmenite cumulates. *Meteorit. Planet. Sci.* **35**, 783–794.

Wagner T. P. and Grove T. L. (1997) Experimental constraints on the origin of lunar high-Ti ultramafic glasses. *Geochim. Cosmochim. Acta* **61**, 1315–1327.

Walker D., Longhi J., Stolper E. M., Grove T. L. and Hays J. F. (1975) Origin of tianiferous lunar basalts. *Geochim. Cosmochim. Acta* **39**, 1219–1235.

Weyer S. and Ionov D. A. (2007) Partial melting and melt percolation in the mantle: the message from Fe isotopes. *Earth Planet. Sci. Lett.* **259**, 119–133.

Weyer S. and Schwieters J. B. (2003) High precision Fe isotope measurements with high mass resolution MC-ICPMS. *Int. J. Mass Spectrom.* **226**, 355–368.

Weyer S., Anbar A. D., Brey G. P., Munker C., Mezger K. and Woodland A. B. (2005) Iron isotope fractionation during planetary differentiation. *Earth Planet. Sci. Lett.* **240**, 251–264.

Wiechert U., Halliday A. N., Lee D. C., Snyder G. A., Taylor L. A. and Rumble D. (2001) Oxygen isotopes and the moon-forming giant impact. *Science* **294**, 345–348.

Wieczorek M. A., Jolliff B. L., Khan A., Pritchard M. E., Weiss B. P., Williams J. G., Hood L. L., Righter K., Neal C. R., Shearer C. K., McCallum I. S., Tompkins S., Hawke B. R., Peterson C., Gillis J. J. and Bussey B. (2006) The constitution and structure of the lunar interior. *Rev. Mineral. Geochem.* **60**, 221–364.

Wiesli R. A., Beard B. L., Taylor L. A. and Johnson C. M. (2003) Space weathering processes on airless bodies: Fe isotope fractionation in the lunar regolith. *Earth Planet. Sci. Lett.* **216**, 457–465.

Williams H. M., Peslier A. H., McCammon C., Halliday A. N., Levasseur S., Teutsch N. and Burg J. P. (2005) Systematic iron isotope variations in mantle rocks and minerals: the effects of partial melting and oxygen fugacity. *Earth Planet. Sci. Lett.* **235**, 435–452.

Zheng Y.-F. (1991) Calculation of oxygen isotope fractionation in metal oxides. *Geochim. Cosmochim. Acta* **55**, 2299–2307.

Associate editor: Christian Koeberl